UNIVERSITY OF BIRMINGHAM
University of Birmingham Research at Birmingham

Assessing boron doped $Ba_2In_{1.8}Si_{0.2}O_{5.1}$ as a potential electrolyte for use in ceramic electrolyte fuel cells

Muhammad, Abubakar; Slater, Peter

DOI:
10.1016/j.jssc.2022.123671

License:
Creative Commons: Attribution-NonCommercial-NoDerivs (CC BY-NC-ND)

Document Version
Peer reviewed version

Citation for published version (Harvard):
Muhammad, A & Slater, P 2023, 'Assessing boron doped $Ba_2In_{1.8}Si_{0.2}O_{5.1}$ as a potential electrolyte for use in ceramic electrolyte fuel cells', *Journal of Solid State Chemistry*, vol. 317, 123671.
https://doi.org/10.1016/j.jssc.2022.123671

Link to publication on Research at Birmingham portal

General rights
Unless a licence is specified above, all rights (including copyright and moral rights) in this document are retained by the authors and/or the copyright holders. The express permission of the copyright holder must be obtained for any use of this material other than for purposes permitted by law.

•Users may freely distribute the URL that is used to identify this publication.
•Users may download and/or print one copy of the publication from the University of Birmingham research portal for the purpose of private study or non-commercial research.
•User may use extracts from the document in line with the concept of 'fair dealing' under the Copyright, Designs and Patents Act 1988 (?)
•Users may not further distribute the material nor use it for the purposes of commercial gain.

Where a licence is displayed above, please note the terms and conditions of the licence govern your use of this document.

When citing, please reference the published version.

Take down policy
While the University of Birmingham exercises care and attention in making items available there are rare occasions when an item has been uploaded in error or has been deemed to be commercially or otherwise sensitive.

If you believe that this is the case for this document, please contact UBIRA@lists.bham.ac.uk providing details and we will remove access to the work immediately and investigate.

Download date: 24. Apr. 2024

Assessing Boron doped $Ba_2In_{1.8}Si_{0.2}O_{5.1}$ as a electrolyte for potential use in ceramic electrolyte fuel cells.

Abubakar Muhammad* and Peter Raymond Slater
School of Chemistry, University of Birmingham, Edgbaston, Birmingham, B15 2TT, United Kingdom

*Corresponding Author: Abubakar Muhammad
Email address: axm1510@bham.ac.uk
School of Chemistry, University of Birmingham, Edgbaston, Birmingham, B15 2TT, United Kingdom.

Abstract

Doped perovskite oxides have been widely studied in recent years as potential proton conducting electrolytes for electrochemical devices. One such system, $Ba_2In_2O_5$ transforms from an orthorhombic phase at room temperature to a cubic perovskite phase at high temperature, which results in a dramatic increase in ionic conductivity. In this paper, we report the incorporation of Boron (B) and Silicon (Si) at the Indium (In) cation site ($Ba_2In_{2-x-y}B_xSi_yO_{5+y/2}$) to stabilise the highly conducting cubic phase at room temperature, as well as lower the sintering temperature required. X-ray powder diffraction data of the synthesized powders sintered at 1250 ˚C reveal successful incorporation of Si and B at the In site with maximum solubility of 10 mol% for both, and conductivity measurements show an enhancement upon dopant incorporation. Further enhancement in conductivity was observed in measurements performed under wet $N_{2(g)}$ atmosphere which is attributed to a protonic contribution to the overall ionic conductivity. In summary, the ionic conductivity of all the doped samples was shown to be at least an order of magnitude higher than that of undoped $Ba_2In_2O_5$ with the best performance observed in $Ba_2In_{1.7}B_{0.1}Si_{0.2}O_{5.1}$ composition.

Key words: Oxyanions, doping, SOFC, PCFC, perovskite

1.0 Introduction

The world's requirement for energy has increased dramatically since the start of industrial revolution. This demand coupled with the need to preserve the ecosystem through developing more environmentally friendly sources of energy has galvanized a lot of research into fuel cells, with solid oxide fuel cells (SOFC's) having received significant attention by virtue of their greater fuel flexibility. Nevertheless, large scale commercialization of conventional SOFC's is hampered by the need for high temperature operation (typically greater than 650 ˚C), due to the high activation energy for lattice oxide ion conduction. [1] This gives rise to a new set of material related challenges such as chemical instability of cell components, incompatible thermal expansion between interconnects and prolonged start-up times. [2-5] To lower the operation temperature, protonic ceramic fuel cells (PCFC's) which utilize proton conducting electrolytes are being developed to benefit from lowered activation energy for conduction of protons compared with oxide ions and hence higher ionic conductivity at lower temperatures. [6]

Research into proton conducting materials has been extensively studied since the pioneering study by Iwahara et al., [7] in 1981, which showed that perovskite materials in humid atmosphere demonstrate proton conductivity. Commonly explored materials for this purpose are perovskite – type barium cerate ($BaCeO_3$) and zirconate ($BaZrO_3$). Considering that the ideal perovskite structure has no anion vacancies, doping of the tetravalent B site cation with a trivalent (or divalent) cation provides anion vacancies which can then be filled by hydroxyl ions, allowing for proton conductivity. [8] Gadolinium (III) for example has been doped in $BaCeO_3$ at the Ce site, leading to a reported protonic conductivity in humid atmosphere of 10^{-2} Ωcm^{-1} at 500

˚C. [9] Above this intermediate temperature, electronic and oxide ion conductivity becomes more prevalent. [10] While doped $BaCeO_3$ compounds show high protonic conductivity at intermediate temperature, they are prone to chemical instability in the presence of $CO_{2\,(g)}$, $SO_{2\,(g)}$ and in humid atmospheres. [3, 11] This major disadvantage greatly limits its use in fuel cell applications. Doped $BaZrO_3$ in contrast is shown to have better chemical stability in CO_2 and steam but has rather problematic sintering which leads to high grain boundary resistance and hence, significantly lower total protonic conductivity. [3, 12, 13]

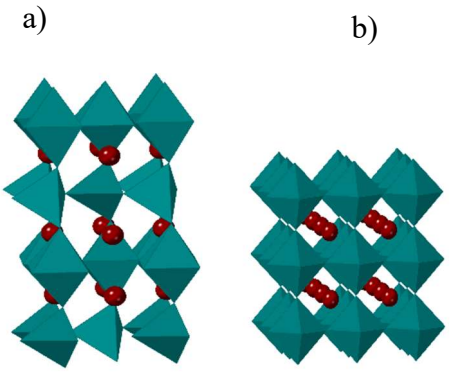

Fig 1: Crystal structure of (a) brownmillerite $Ba_2In_2O_5$ with alternating layers of InO_6 octahedra and InO_4 tetrahedra. (b) perovskite ABO_3 with corner shared BO_6 octahedra

Another perovskite of particular interest is $Ba_2In_2O_5$ (BI) which adopts the orthorhombic brownmillerite structure with alternating sequence of InO_6 octahedra and InO_4 tetrahedra at room temperature (Fig. 1a). This ordering of the oxide ion vacancies gives $Ba_2In_2O_5$ a rather low ionic conductivity at intermediate temperatures. At temperature above 900 ˚C however, the orthorhombic structure transforms to tetragonal resulting in a discontinuous jump in conductivity. On further heating to temperature above 1000 ˚C, the structure becomes cubic (Fig. 1b) with oxide ion vacancies totally disordered leading to high ionic conductivity. This has motivated a lot of research to stabilize the highly conducting cubic phase at room temperature, which has mainly been by aliovalent doping of the In site with cations of similar size. [14-18] More recently, Shin et al., [19] successfully stabilized the disordered cubic perovskite phase by silicate incorporation and observed significant enhancement of conductivity at 400 ˚C in $Ba_2In_{1.8}Si_{0.2}O_{5.1}$ under humid atmosphere. Further ^{29}Si NMR and Raman spectroscopic analysis revealed that Si was incorporated into the lattice as a tetrahedral group (SiO_4^{4-}) which explains why detrimental silica aggregates did not form at the grain boundaries as was previously observed for other fuel cell materials. [20, 21] At first glance the incorporation of such a smaller Si^{4+} in place of In^{3+} (ionic radii (CN=4) In^{3+} 0.62Å, Si^{4+} 0.26Å) might seem surprising, but it has been shown particularly in the work on cuprate superconductors in the late 80s/early 90s that the perovskite structure can accommodate such small dopants. In this work, it was shown that even smaller dopants such as carbonate and borate could be incorporated (see for example the review article [22]). As noted in this review, it is likely that there are significant localised distortions to accommodate these dopants.

Our aim in this work was to attempt to co-dope $Ba_2In_{2-x}Si_xO_{5+x/2}$ to overcome the need for very high temperatures >1400 ˚C to obtain suitably sintered electrolyte membranes. [19] To achieve this, we here investigated co-doping of Boron. Boron was chosen as it has been shown to be able to be accommodated into perovskite-type cuprates (such as $LaBaCuBO_5$) [23], and it is an isovalent dopant and so would not change the oxygen content. Furthermore, it was expected that boron would help to enhance the sintering of the samples. The results show that, not only do the samples sinter at lower temperatures but also show appreciable protonic conductivity.

2.0 Materials and Methods

Si and B doped samples: $Ba_2In_2O_5$, (BI); $Ba_2In_{1.8}Si_{0.2}O_{5.1}$ (BIS2); $Ba_2In_{1.7}B_{0.1}Si_{0.2}O_{5.1}$, (BIB1S2); $Ba_2In_{1.6}B_{0.2}Si_{0.2}O_{5.1}$, (BIB2S2); $Ba_2In_{1.6}B_{0.3}Si_{0.1}O_{5.05}$, (BIB3S1) and $Ba_2In_{2-x-y}B_xSi_yO_{5+y/2}$, (BIB4S2) were synthesized by weighing and mixing stoichiometric amounts of $BaCO_3$ (99.8 %), In_2O_3 (99.9 %), H_3BO_3 (99.8 %) and SiO_2 (99.5 %) via the solid state synthesis route. Excess 3% $BaCO_3$ was added in order to compensate for the effect of BaO loss at elevated temperature without which barium deficient impurity phase such as $BaIn_2O_4$ is detected in the XRD pattern of the prepared samples. [24] The powders were intimately ground and heated initially to 1000 ºC for 12 hrs before being ball milled at 500 rpm for 30 mins using Fritsch Pulverisette 7 Planetary Mill (zirconia balls and jars) and reheated at 1000 ˚C for 12 hrs. 1g of each sample was pressed into cylindrical pellet of 13mm in diameter and covered in sample powder in order to limit BaO loss at the pellet surface. The crucible was then covered with lid and calcined at 1200 ºC for 12 hrs and 1250 ˚C for another 12hrs with intermediate grinding and homogenizing of the sample powder.

Sample phase purity was determined from the powder X-ray Diffraction (PXRD) pattern of the sintered powders, which was carried out on Bruker D8 diffractometer equipped with Cu Kα (1.5406 Å) radiation. For detailed structural and unit cell parameters, GSAS II Rietveld refinement software [25] was used. Raman Spectroscopy measurements were made on a Renishaw inVia Raman microscope with excitation using Cobalt Samba CW 532 nm green laser and the sample microstructure was examined using a Hitachi TM4000Plus tabletop electron microscope

For hydration studies, sample powders were heated in a tube furnace in an atmosphere of N_2 gas bubbled through deionized water at room temperature. The samples were heated to 600 ˚C then held for 3 hrs and slow cooled at rate of 0.4 ˚C /min to room temperature. The water content from hydrated samples was determined using Thermogravimetric analysis on a Netzsch STA 449 F1 Jupiter Thermal Analyzer coupled with Netzsch MS 403C Aëolos Mass Spectrometer. Samples of 50-60 mg were heated at a rate of 10 ºC/min to 700 ºC in N_2 and the water content was calculated from the mass loss.

For conductivity measurements, sintered pellets of > 80 % theoretical density pellets were polished with sand paper and coated with gold paste on each of the two faces. Two gold wires were attached on either side of each pellet then heated to 850 ˚C for 1 hr to ensure bonding to the pellet. Conductivity measurements were then carried out on a Hewlett Packard 4182A Impedance Analyser in the frequency range 0.1-10^7 Hz and temperature range of 300-750 ˚C. The impedance data were analysed using equivalent circuits fitting on Zview software. For each sintered pellet, two sets of measurements were made. The first measurement was set up in dry atmosphere in which N_2 gas (to eliminate any p-type contribution to the conductivity) was bubbled through concentrated sulphuric acid to obtain oxide ion conductivity. The second measurement was performed under wet atmosphere in which N_2 gas was bubbled through deionized water. This measurement was made in order to identify protonic contribution to the overall conductivity.

3.0 Results and Discussion

Powder X-ray Diffraction (PXRD) patterns (collected at RT) of the as-synthesized samples were obtained after heating the prepared samples at 1000 ˚C, 1200 ˚C and 1250 ˚C to investigate the phase formation and to determine the solubility limit of the dopants. It was previously reported that the maximum solubility limit of silicate in $Ba_2In_2O_5$ is 10 mol%. Above this percentage, Ba_2SiO_4 impurities were observed. [19] The X-ray diffraction patterns of the doped samples showed some elements of cubic phase formed at 1000 ˚C albeit with significant impurity peaks (Fig. 2a) suggesting the need for further heating to higher temperature

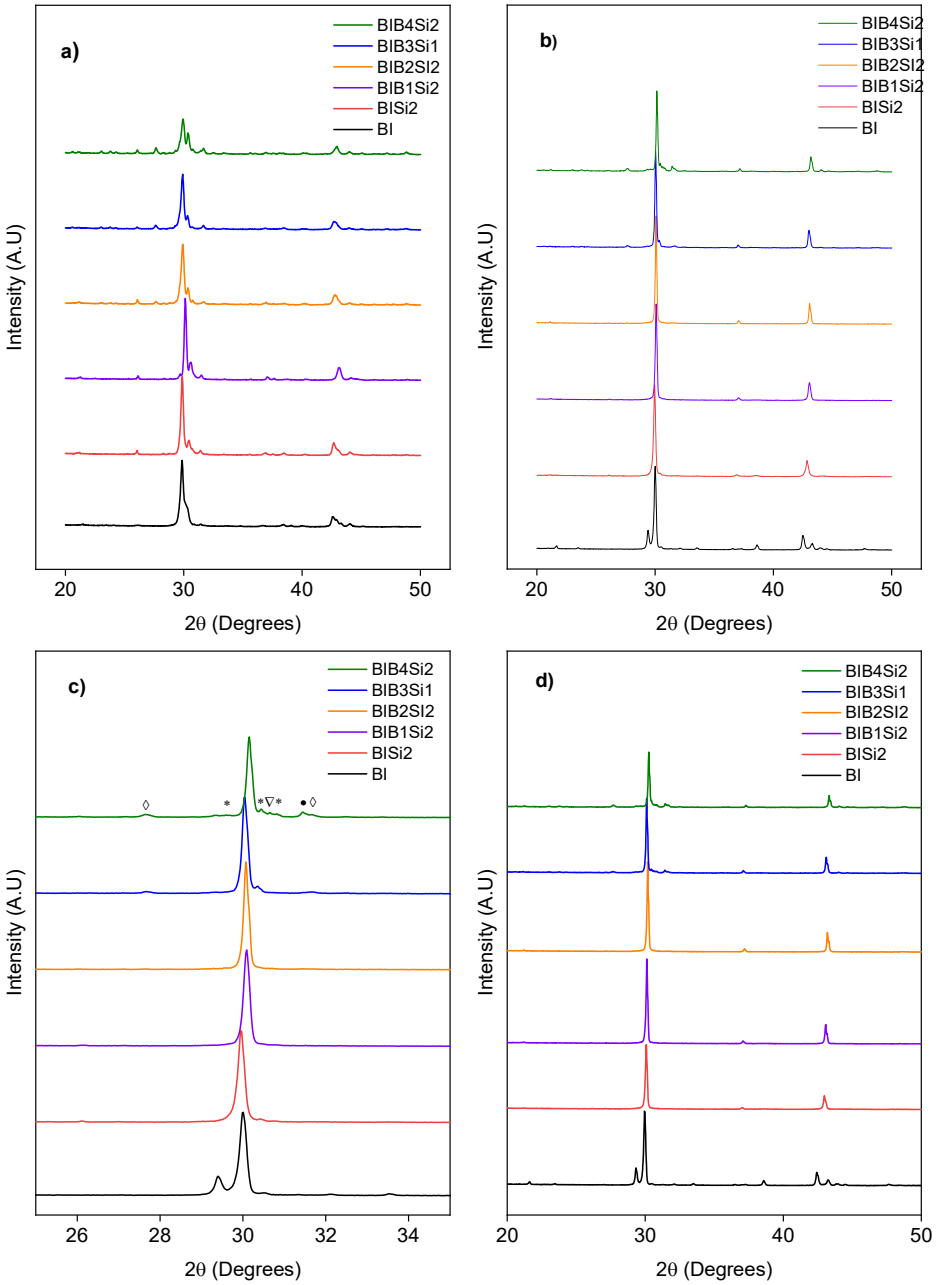

Fig. 2: Room temperature X-ray powder diffraction pattern of $Ba_2In_{2-x-y}B_xSi_yO_{5+y/2}$ heated at a) 1000 ˚C, b) 1200 ˚C and c) Expanded region of Fig. 2b (1200 ˚C) to illustrate the impurity peaks in region 25 -35 degrees. (◊ denotes $Ba_3(BO_3)_2$ peak positions; * Ba_2SiO_4; ∇ In_2O_3 and ● $BaIn_2O_4$). d) 1250 ˚C

By further heating the samples to 1200 °C (Fig. 2b), samples with small borate content BIB1S2 and BIB2S2 were shown to be single phase cubic. Samples with higher Borate content BIB3S1 and BIB4S2 on the other hand, although appearing to be still cubic, still showed $Ba_3(BO_3)_2$, In_2O_3 and $BaIn_2O_4$ peaks. These impurity peaks were still persistent even after heating to 1250 °C (Fig 3c), ultimately suggesting that the maximum solubility limit of B in the $Ba_2In_{2-x-y}B_xSi_yO_{5+y/2}$ is 10 mol%. Above this limit the excess borate reacts with Barium carbonate to form barium borate thereby additionally creating the barium deficient impurities $BaIn_2O_4$ and In_2O_3. The undoped sample BI showed an orthorhombic cell at 1200 °C consistent with expected XRD pattern of brownmillerite $Ba_2In_2O_5$ structure reported previously. [18, 26-28] A small amount of impurity was also observed on the silicate only doped sample BIS2 prompting the need to heat to even higher temperature in order to obtain a single phase sample without B doping.

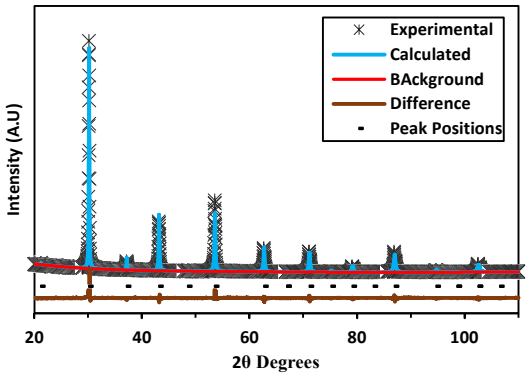

Fig. 3: Observed, calculated and difference X-ray diffraction profiles for BIB2S2

Fig. 2c shows X-ray Diffraction patterns of the samples heated at 1250 °C. Doped samples with lower boron content BIB1S2 and BIB2S2 showed pure cubic perovskite pattern while the undoped sample BI retained its orthorhombic brownmillerite phase as expected. Samples doped with higher boron content BIB3S1 and BIB4S2 showed impurity peaks similar to those obtained at 1200 °C. This confirms that the pure cubic phase cannot be obtained for these higher B compositions even after heating to higher temperatures thus indicating that the borate doping limit had been exceeded. Another thing to note is that at a heating temperature of 1250 °C, BIB3S1 and BIB4S2 begin to show partial melting particularly for the highest B content sample, BIB4S2. This does however suggest that borate incorporation is successful in reducing the sintering temperature of doped barium indate samples in comparison to other reported dopants. [29-31] Complementing the PXRD results, RT Raman spectra of the doped samples were similarly collected for samples prepared at the different synthesis temperatures. It could be seen that for the 1000 °C synthesised samples (Fig. 5a), the carbonate peaks of $BaCO_3$ of the reactant mixture is already eliminated for samples doped with Borate. However, BI and BIS2, which both have no borate showed two distinct carbonate vibrations:one at 1050 cm^{-1} attributed to Ruddlesden Popper intermediate carbonate phase ($Ba_4In_2O_6CO_3$) [32] and another at 1075 cm^{-1} from unreacted $BaCO_3$. Both carbonate peaks disappeared upon heating to 1200 °C as the pure phase forms. This lower temperature elimination of carbonate is probably related to borate lowering the synthesis temperature for the perovskite phase.

Table 1: Refined unit cell parameters of $Ba_2In_{2-x-y}B_xSi_yO_{5+y/2}$ (prepared at 1250 °C).

Doping Level	Composition	Unit Cell Parameters (Å)			Unit Cell Volume (Cubic cell equivalent) (Å^3)	Space group
		a	b	c		
BI	$Ba_2In_2O_5$	6.0845(5)	16.723(1)	5.9563(5)	606.087 (75.76)	*I b m 2*
BISi2	$Ba_2In_{1.8}Si_{0.2}O_{5.1}$	4.2211(2)	4.2211(2)	4.2211(2)	75.2102	*P m* $\bar{3}$ *m*
BIB1Si2	$Ba_2In_{1.7}B_{0.1}Si_{0.2}O_{5.1}$	4.1995(2)	4.1995(2)	4.1995(2)	74.0615	*P m* $\bar{3}$ *m*
BIB2Si2	$Ba_2In_{1.6}B_{0.2}Si_{0.2}O_{5.1}$	4.1848(2)	4.1848(2)	4.1848(2)	73.2865	*P m* $\bar{3}$ *m*

Rietveld refinement was performed for samples in which pure phases were obtained (BI, BIS2 BIB1S2 and BIB2S2 synthesised at 1250 °C). An example Rietveld refinement fit (for BIB2S2) is shown in (Fig. 3) and the refined cell parameters for all the samples are shown in Table 1. The undoped BI powder was refined using the *Ibm2* orthorhombic space group (ICSD collection code: 73937), while the doped samples were refined with the *Pm-3m* space group (ICSD collection code: 48208). Figure 4 shows the variation of the equivalent unit cell volume upon borate and silicate doping (Fig. 4). Incorporation of silicate (BIS2) reduced the unit cell volume compared to a cubic equivalent of BI undoped unit cell which can be attributed to the smaller ionic radius of Si^{4+} compared to In^{3+}. Thus, despite the higher oxygen content on Si doping, this is not sufficient to cancel out the effect of replacing In^{3+} by the smaller Si^{4+}.

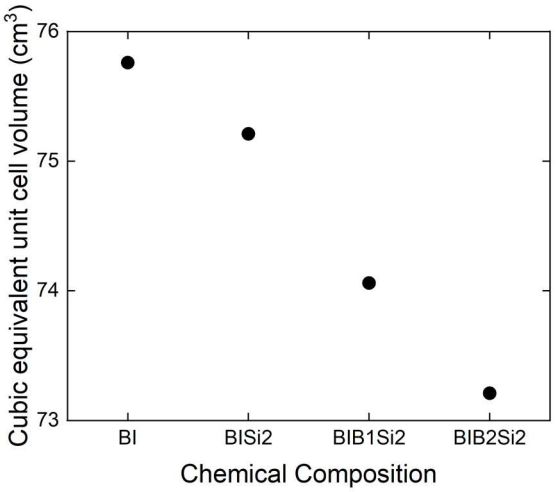

Fig. 4: Variation of unit cell volume with Si and B dopant incorporation

Incorporation of borate alongside silicate resulted in a further decrease in unit cell volume, which again can be related to the smaller B^{3+} dopant size compared to In^{3+} . This adds further support for the successful incorporation of B in addition to Si

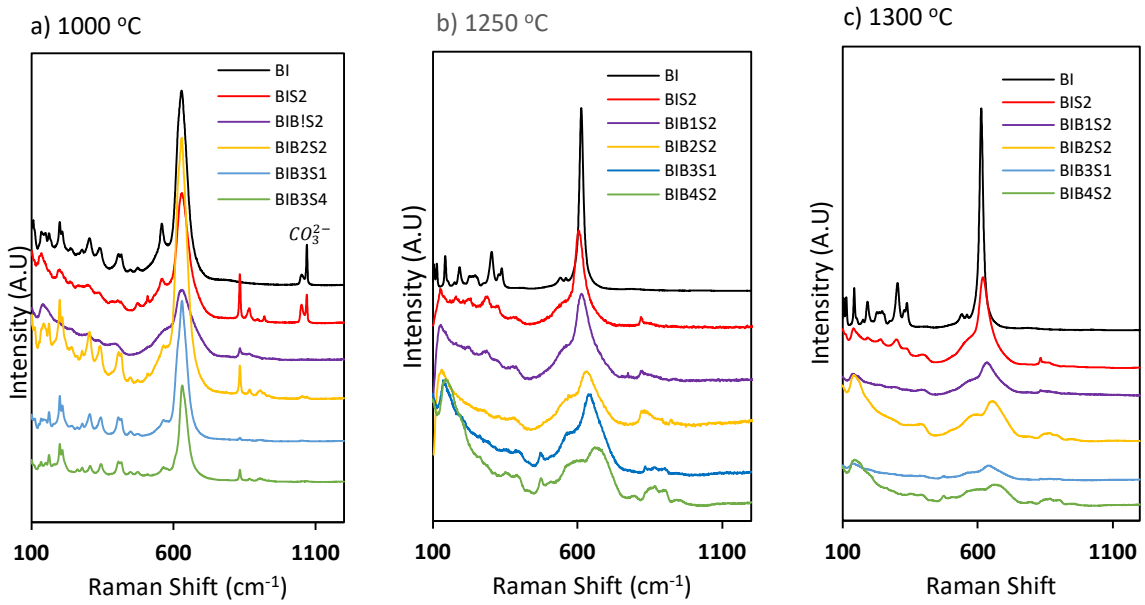

Fig. 5: Room temperature Raman spectra $Ba_2In_{2-x-y}B_xSi_yO_{5+y/2}$ sintered at a) 1000 °C, b) 1200 °C and c) 1250 °C. Carbonate peaks highlighted

Fig. 5a shows the Raman spectra of the samples prepared at 1000 ˚C. The data show a decrease in intensity of the In-O band around 600-650 cm^{-1} for the doped samples consistent with a transition towards cubic symmetry. Furthermore, Si doped samples show emergence of peaks due to Si - O around 830 cm^{-1} consistent with the presence of tetrahedrally co-ordinated Si. [33] The spectra obtained at 1200 ˚C and 1250 ˚C (Fig 5b and c) demonstrate general flattening of the bands along with shifting of the In – O vibrations to higher frequency for the B doped samples. This significant reduction in peak intensity is consistent with the formation of a cubic perovskite phase which ideally has no Raman bands. [34, 35] The observation of some Raman bands in the spectra however, indicates a degree of local distortion from ideal cubic symmetry in spite of the average structure being cubic (as determined from the PXRD pattern earlier Fig. 2c).

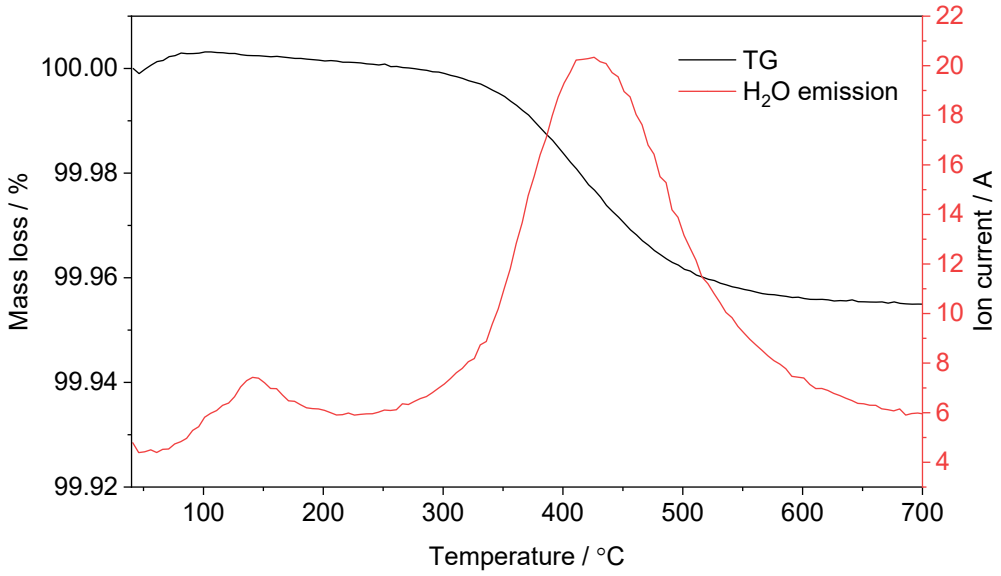

Fig. 6: TG/MS data of BIB2S2 in the temperature range 40-700 ˚C showing the thermogravimetric mass loss (Black line), mass spectrometric ion current of H_2O (Red lines).

Table 2: Water content of $Ba_2In_{2-x-y}B_xSi_yO_{5+y/2}$. samples obtained from thermogravimetric analysis of hydrated powders.

Sample composition	**Composition**	**Water of Hydration (mol)**
BI	$Ba_2In_2O_5$	0.9 ± 0.02
BIS2	$Ba_2In_{1.8}Si_{0.2}O_{5.1}$	0.6 ± 0.03
BIB1S2	$Ba_2In_{1.7}B_{0.1}Si_{0.2}O_{5.1}$	0.5 ± 0.03
BIB2S2	$Ba_2In_{1.6}B_{0.2}Si_{0.2}O_{5.1}$	0.4 ± 0.05

To investigate water incorporation into the powders in wet N_2, Thermogravimetric and Powder X-ray diffraction analysis was performed on the hydrated powders. As an example, the TGA profile of hydrated BIB2S2 is shown in Fig. 6. This shows a small loss of surface water at temperature of 80 – 170 ˚C, along with a larger water loss in the range 300-600 ˚C due to bulk water. TG mass loss corresponding to surface water loss was not included in the calculation of water content. This temperature range corresponds to the temperature at which protonic mobility is maximum. [16] The amount of water incorporated into each sample was calculated from an average of 3 TGA experiments (Table 2). It can be seen that undoped $Ba_2In_2O_5$ has the highest amount of water intake, with a value (0.9 ± 0.02) close to 1 H_2O per formulas unit as expected. This indicates near complete filling of the oxide ion vacancies by hydroxide in this compound. Silicate incorporation reduces the amount of water intake to 0.6 ± 0.03 for BIS2. This lowering of water incorporation can be attributed to both a lower level of oxide ion vacancies as well as the inability to fill vacancies around the silicate oxyanion. Hydrated samples with borate incorporated alongside silicate (BIB1S2 and BIB2S2)

shows a further decrease in the amount of water content, which can be attributed to the inability to accommodate water around the borate groups as well.

Table 3: Refined unit cell parameters of $Ba_2In_{2-x-y}B_xSi_yO_{5+y/2}.nH_2O$ hydrated powders

Doping Level	Solid Solution	Lattice Parameters (Å)			Unit Cell Volume (Cubic equivalent) (Å^3)	Space group
		a	b	c		
x = 0; y = 0	$Ba_2In_2O_5$	4.17(6)	4.17(6)	9.00(0)	156.9 (78.5)	*P 4/m m m*
x = 0; y = 0.2	$Ba_2In_{1.8}Si_{0.2}O_{5.1}$	4.18(9)	4.18(9)	8.79(8)	154.3 (77.2)	*P 4/m m m*
x = 0.1; y = 0.2	$Ba_2In_{1.7}B_{0.1}Si_{0.2}O_{5.1}$	4.22(8)	4.22(8)	4.22(8)	75.59	*P m* $\bar{3}$ *m*
x = 0.2; y = 0.2	$Ba_2In_{1.6}B_{0.2}Si_{0.2}O_{5.1}$	4.18(7)	4.18(7)	4.18(7)	73.44	*P m* $\bar{3}$ *m*

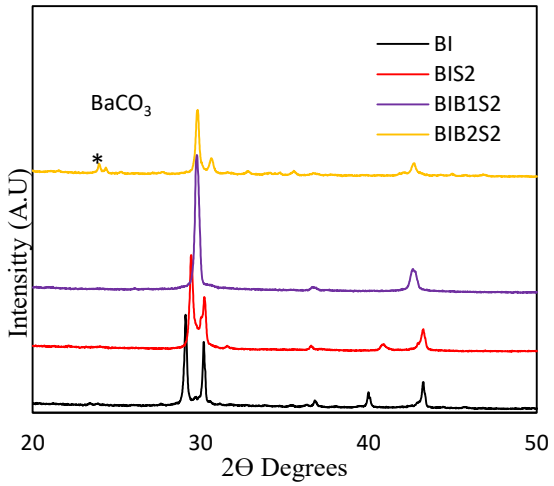

Fig. 7: Room temperature X-ray Diffraction Patterns of hydrated $Ba_2In_{2-x-y}B_xSi_yO_{5+y/2}$ powders

In addition to Thermogravimetric analysis, X-ray Powder diffraction data were also collected for the hydrated powders. The refined cell parameters for these hydrated samples are shown in Table 3. From these results (Fig 7, Table 3) it can be seen that water incorporation leads to structural change of undoped BI from an orthorhombic I*bm2* to a tetragonal P*4/mmm* cell. Hydrated BIS2 is also shown to adopt a similar tetragonal *P4/mmm* cell, albeit with reduced tetragonal distortion. In contrast, the borate doped samples BIB1S2 and BIB2S2 all retained their cubic structure after water incorporation. However, the powder of the lower B content sample, BIB1S2, shows some evidence of partial decomposition with $BaCO_3$ peaks observed in the diffraction pattern (Fig. 7). All unit cell volumes were shown to expand on water uptake as expected. The

level of expansion for each cell in comparison to anhydrous powder is shown in Fig. 8. From these data, it is apparent that the trend in unit cell expansion is similar to the trend obtained from amount of water incorporated. BI incorporated the highest amount of water and thus has the largest equivalent unit cell volume expansion, while BIB2S2 has the smallest water incorporation and hence smallest volume expansion.

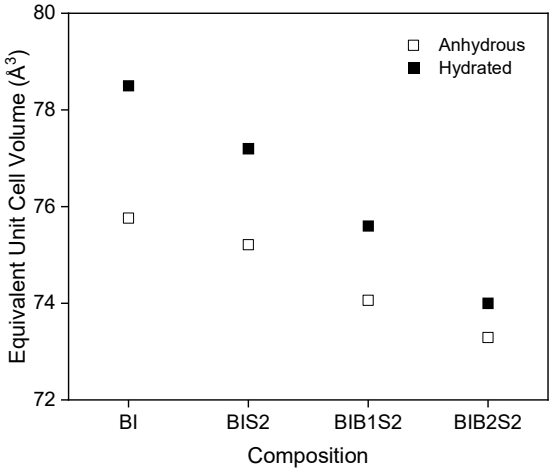

Fig. 8: Comparison of unit cell volumes of hydrated and anhydrous $Ba_2In_{2-x-y}B_xSi_yO_{5+y/2}$ powders, showing reducing expansion on water incorporation of Si and B doping

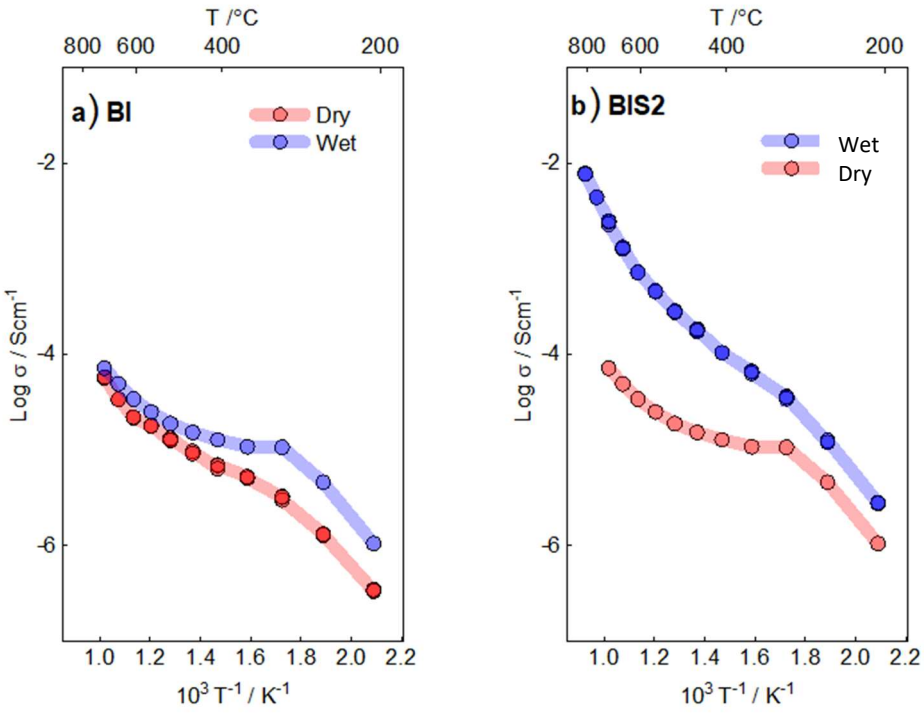

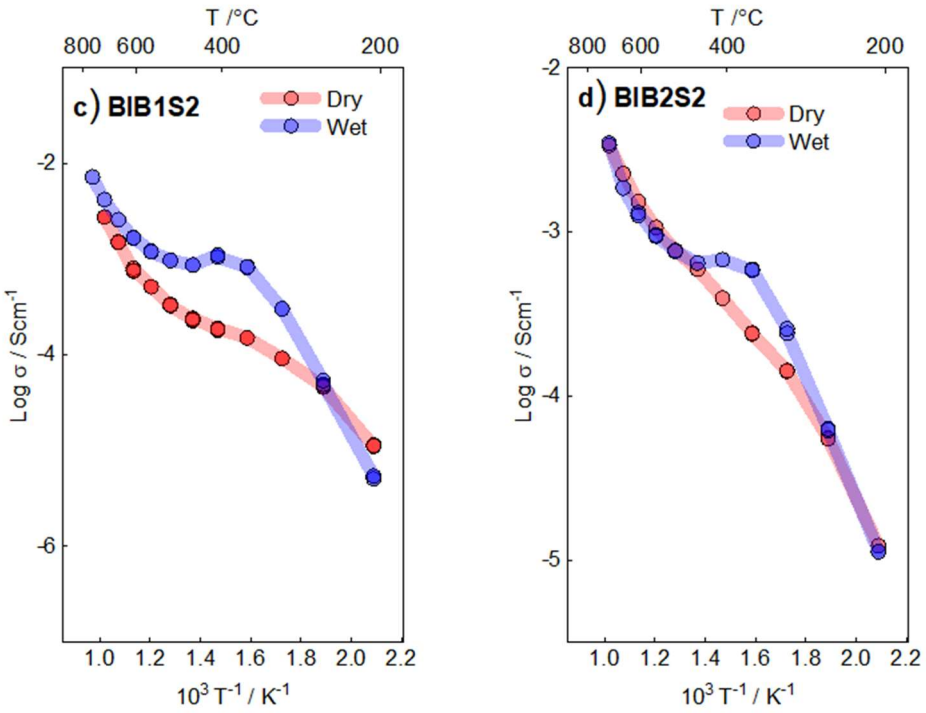

Fig. 9: Arrhenius plots of conductivities of $Ba_2In_{2-x-y}B_xSi_yO_{5+y/2}$ in Dry N_2 (Red lines) and Wet N2 (Blue lines)

Table 4: Conductivity data for $Ba_2In_{2-x-y}B_xSi_yO_{5+y/2}$

Sample composition	Conductivity at 400 ˚C (Scm^{-1})	
	Wet N_2	Dry N_2
BI	1.316×10^{-5}	6.18×10^{-6}
BIS2	1.02×10^{-4}	9.67×10^{-5}
BIB1S2	1.05×10^{-3}	1.76×10^{-4}
BIB2S2	6.52×10^{-4}	3.29×10^{-4}

Having demonstrated successful incorporation of B and Si, the effect of this doping strategy on the protonic conductivity was investigated in Fig 9 with the data in wet N_2 (blue lines) showing the highest conductivity values indicative of the protonic contribution to the conductivity. The conductivity measurement at low temperature indicate a substantial increase with dopant incorporation. Thus at 400 ºC, incorporation of 5 % B and 10 % Si leads to an increase in conductivity by 2 orders of magnitude compared to undoped $Ba_2In_2O_5$ (Table 1). The increase in conductivity can be attributed to the stabilization of the cubic perovskite phase

with disordered oxygen vacancies. At temperatures above 400 ˚C, elimination of water from the lattice reduces the protonic contribution to overall conductivity and hence the deviation from linearity in the conductivity plots is observed. The microstructure of the sintered pellets was examined by SEM (Fig 10). This reveals a fairly dense pellet with occasional pin holes. The pin holes are especially visible for undoped BI, which also showed evidence of cracking, which may relate to strains induced by the order-disorder structural changes at elevated temperatures

.

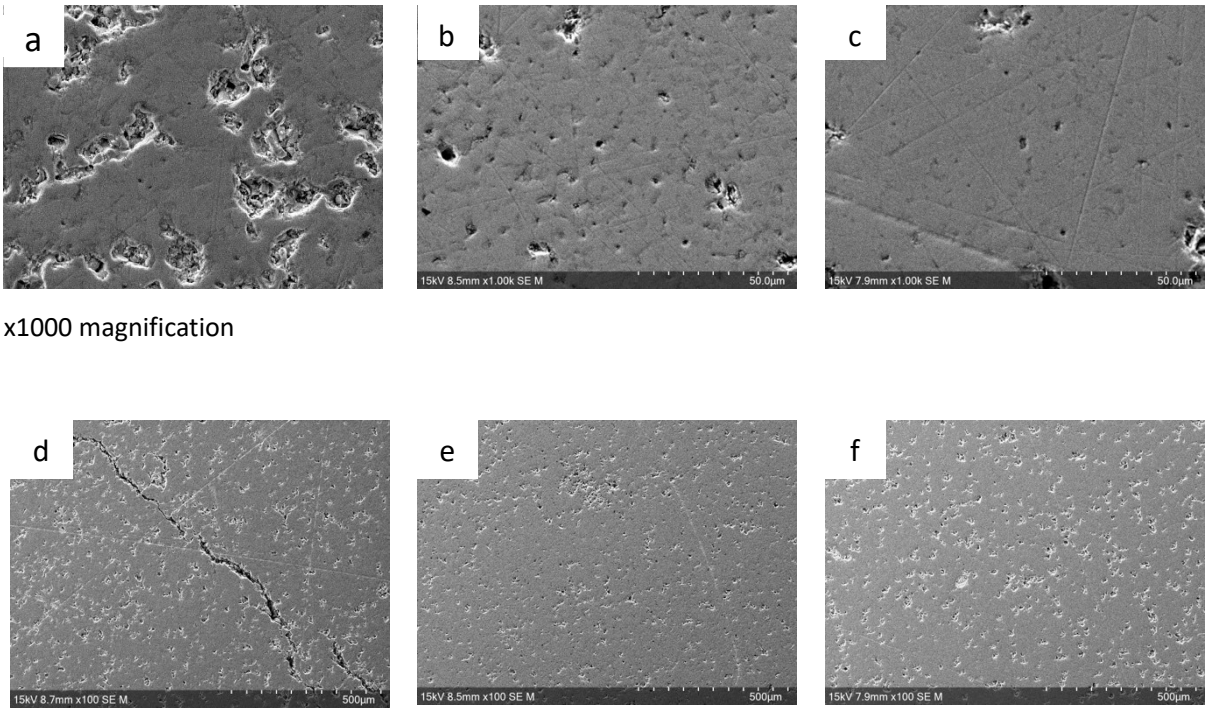

Fig. 10: Scanning electron micrograph of BI, BIB1S2 and BIB2S2 respectively showing morphology of the sintered pellets a), b) and c): x1000 magnification; d), e) and f): x100 magnification

5.0 Conclusions

In summary, the synthesis, characterization, and proton conductivities in $Ba_2In_{2-x-y}B_xSi_yO_{5+y/2}$ have been reported. It is shown that incorporation of Si is successful in transforming the brownmillerite structure of $Ba_2In_2O_5$ with ordered anion vacancies to a disordered cubic perovskite structure resulting in increase in ionic conductivity. Co-doping of B in the structure was influential in reducing the sintering temperature to 1250 ˚C in addition to further increase in the ionic conductivity. B doping is also shown to suppress the transformation to a tetragonal cell on hydration. The conductivity was predominantly protonic in wet N_2 at

lower temperature with maximum conductivity for BIB1S2 (1.05 x 10^{-3} Scm^{-1} at 400 ˚C). In conclusion, our research suggests that co-doping with B and Si is beneficial for the sintering and conductivity in $Ba_2In_2O_5$.

6.0 Acknowledgements

The authors would like to thank the Petroleum Technology Development Fund Nigeria (PTDF) for the PhD grant obtained through their UK Overseas Postgraduate Scholarship Program.

7.0 References

1. Y. Zhang, R. Knibbe, J. Sunarso, Y. Zhong, W. Zhou, Z. Shao and Z. Zhu, *Adv Mater*, 2017, **29**, 1700132-1700165.
2. A. Lashtabeg and S. J. Skinner, *J Mater Chem*, 2006, **16**, 3161-3170.
3. E. Fabbri, D. Pergolesi and E. Traversa, *Chem Soc Rev*, 2010, **39**, 4355-4369.
4. Y. Liu, L. Fan, Y. Cai, W. Zhang, B. Wang and B. Zhu, *ACS Appl Mater Interfaces*, 2017, **9**, 23614-23623.
5. L. Fan, B. Zhu, P.-C. Su and C. He, *Nano Energy*, 2018, **45**, 148-176.
6. R. Ren, Z. Wang, C. Xu, W. Sun, J. Qiao, D. W. Rooney and K. Sun, *Journal of Materials Chemistry A*, 2019, **7**, 18365-18372.
7. H. Iwahara, T. Esaka, H. Uchida and N. Maeda, *Solid State Ionics*, 1981, **3-4**, 359-363.
8. N. Zakowsky, S. Williamson and J. Irvine, *Solid State Ionics*, 2005, **176**, 3019-3026.
9. S. M. Haile, G. Staneff and K. H. Ryu, *J Mater Sci*, 2001, **36**, 1149-1160.
10. N. Fukatsu, T. Kurita, K. Yajima, K. K and J. Ohashi, *Journal of Alloys and Compounds*, 1995, **231**, 706.
11. A. Łącz and P. Pasierb, *J Therm Anal Calorim*, 2013, **113**, 405-412.
12. P. Babilo and S. M. Haile, *J Am Ceram Soc*, 2005, **88**, 2362-2368.
13. F. A. de Bruijn, V. A. T. Dam and G. J. M. Janssen, *Fuel Cells*, 2008, **8**, 3-22.
14. K. R. Kendall, C. Navas, J. K. Thomas and H. C. zurLoye, *Solid State Ionics*, 1995, **82**, 215-223.
15. P. Berastegui, S. Hull, F. J. García-García and S. G. Eriksson, *Journal of Solid State Chemistry*, 2002, **164**, 119-130.
16. E. Quarez, S. Noirault, M. T. Caldes and O. Joubert, *Journal of Power Sources*, 2010, **195**, 1136-1141.
17. S. Noirault, E. Quarez, Y. Piffard and O. Joubert, *Solid State Ionics*, 2009, **180**, 1157–1163.
18. D. Gregory and M. Weller, *Phases in the System Ba2M2-xCuxO4+δ, M = In, Sc: Structure and Oxygen Stoichiometry*, 1993.
19. J. F. Shin, D. C. Apperley and P. R. Slater, *Chemistry of Materials*, 2010, **22**, 5945-5948.
20. N. Schrödl, E. Bucher, C. Gspan, A. Egger, C. Ganser, C. Teichert, F. Hofer and W. Sitte, *Solid State Ionics*, 2016, **288**, 14-21.
21. Z. Yang, M. Guo, N. Wang, C. Ma, J. Wang and M. Han, *Int J Hydrogen Energ*, 2017, **42**, 24948-24959.

22. C. A. Hancock, J. M. Porras-Vazquez, P. J. Keenan and P. R. Slater, *Dalton Transactions*, 2015, **44**, 10559-10569.
23. L. Rukang, R. K. Kremer and J. Maier, *Journal of Solid State Chemistry*, 1993, **105**, 609-612.
24. J. F. Shin, A. Orera, D. C. Apperley and P. R. Slater, *J Mater Chem*, 2011, **21**, 874-879.
25. B. H. Toby and R. B. Von Dreele, *J Appl Crystallogr*, 2013, **46**, 544-549.
26. S. Speakman, *Solid State Ionics*, 2002, **149**, 247-259.
27. C. A. J. Fisher and M. S. Islam, *Solid State Ionics*, 1999, **118**, 355-363.
28. G. B. Zhang and D. M. Smyth, *Solid State Ionics*, 1995, **82**, 161-172.
29. L. Zhang, J. Meng, F. Yao, W. Zhang, X. Liu, J. Meng and H. Zhang, *Inorg Chem*, 2018, DOI: 10.1021/acs.inorgchem.8b01853.
30. T. Yao, Y. Uchimoto, M. Kinuhata, T. Inagaki and H. Yoshida, *Solid State Ionics*, 2000, **132**, 189-198.
31. A. Rolle, G. Fafilek and R. N. Vannier, *Solid State Ionics*, 2008, **179**, 113-119.
32. J. Deakin, I. Trussov, A. Gibbs, E. Kendrick and P. R. Slater, *Dalton Trans*, 2018, **47**, 12901-12906.
33. J. F. Shin, K. Joubel, D. C. Apperley and P. R. Slater, *Dalton Trans*, 2012, **41**, 261-266.
34. M. Karlsson, A. Matic, C. S. Knee, I. Ahmed, S. G. Eriksson and L. Börjesson, *Chemistry of Materials*, 2008, **20**, 3480-3486.
35. I. Ahmed, S. Eriksson, E. Ahlberg, C. Knee, P. Berastegui, L. Johansson, H. Rundlof, M. Karlsson, A. Matic and L. Borjesson, *Solid State Ionics*, 2006, **177**, 1395-1403.